

Novel reconfigurable walking machine tool enables symmetric and non-symmetric walking configurations

Josue Camacho-Arreguin, Mingfeng Wang, Matteo Russo, Xin Dong, Dragos Axinte

Abstract—Current research on walking robots strives to achieve a higher efficiency, a better load capacity and an increased adaptability. Parallel Kinematic Manipulators (PKMs) are characterized by high payload and accuracy, but conventional PKMs with fixed configurations are limited to constrained workspaces in known structured environments. In this paper, we propose a parallel Reconfigurable Walking Machine Tool that overcomes these limits by adapting its configuration and gaits to different scenarios. A lightweight and compact positioning system with shape memory alloy actuation is presented to achieve reconfiguration capabilities. Furthermore, kinematic, stability and force analyses are reported to determine the optimal walking gaits in three different scenarios (with inclined slopes at different angles) and four robot configurations. Finally, a set of experiments with the physical prototype validates the proposed models. The results show that symmetric configurations present a better performance at lower ground inclinations (0.5% error), whilst asymmetric configurations can climb on slope conditions that would prevent the use of conventional PKMs (18% or 10°).

Index Terms—Gait analysis, reconfigurable parallel kinematic machine, walking robot, machine tool.

I. INTRODUCTION

CURRENT research on walking robots has extensively relied on nature-inspired mechanisms (e.g. mammals, insects, reptiles) in search of efficiency, higher payload and gait adaptability [1]. For instance, mammal-inspired walking robots can transport heavy loads at high walking speeds thanks to their vertically configured legs [2]. Conversely, insect-inspired robots (e.g. hexapods) can traverse complicated terrains, as they can maintain three or more limbs in contact with the ground at any time, with higher stability coefficients than bipeds and quadrupeds. Thus, the number, distribution, and configuration of the legs play a crucial role in the performance of walking robots (e.g. speed, stability coefficients, actuation torque, etc.). Currently, most walking robots are based on fixed configurations, selected according to desired environments and walking conditions. As such, their performance is hindered if the conditions are not ideal. Further, industrial applications of walking robots require operational capabilities (e.g. inspection, machining, repair, etc.), that usually need multiple additional degrees of freedom (DoF). Hence, they need not only walking but also manipulation capabilities.

Parallel Kinematic Machines (PKMs) are appealing for both walking and operation thanks to their high rigidity and precision [3]-[5]. From an operational perspective, PKMs have been proved to be reduce manufacturing times and improving final product quality in industrial applications (e.g. aerospace [6], energy [7], precision machining [8]-[11], grasping [12]). The higher performance also benefits locomotion, as shown by multiple examples of robotic legs with parallel architectures [13]-[18]. However, their inherent disadvantages, such as complex kinematics and a reduced workspace when compared to the PKM's size still limit their applications.

Reconfigurable PKMs overcome some of these limitations, enhancing capabilities by adapting their configuration for different operational requirements, providing a clear advantage against their conventional counterparts [19]-[24]. For example, PKMs are affected by singularities in their workspace, constraining operation to small singularity-free regions; an adaptive PKM can instead adapt its workspace to avoid singularities for a desired task [25]. From a locomotion perspective, this adaptability can be used to overcome obstacles or enhance walking performance [26][27]. In [26], an optimal hexapod limb distribution is computed to reduce the forces exerted on the limbs on flat terrain in a tripod gait. Similarly, the hexapod in [28] can reconfigure to improve its stability, climbing capabilities and energy consumption.

While these studies prove the advantages of reconfigurable PKM, the focus is on improving performance on either walking or operation only. However, a mechanism able to perform both locomotion and manipulation has clear benefits both in terms of cost and operation, as shown in the examples in [29]-[32]. In [29], a 6-DoF PKM based quadruped robot is introduced for both manufacturing and locomotion in large workspaces; other PKMs capable of both walking and machining are proposed in [30][31]. However, as these robots require external intervention for pose referencing (e.g. clamping pins in [29]), autonomous use is prevented in unprepared environments. Conversely, the 6-DoF PKM hexapod in [32] is capable of walking in unstructured environments [33] and achieve high precision machining after an autonomous calibration [34][35].

This research builds on previous studies on an adaptive PKM with both machining and walking capabilities [32]-[35]. This combined operation is particularly challenging, as high-precision machining imposes constraining requirements for operation that can significantly affect the walking capabilities

Submitted for review on 22/09/2021.

This work was supported in part by UK EPSRC project Robotics and Artificial Intelligence in Nuclear (RAIN) under grant EP/R026084/1.

The authors are with the Department of Mechanical, Materials and Manufacturing Engineering at the University of Nottingham NG7 2RD, U.K. (email: {josue.camachoarreguin; mingfeng.wang; matteo.russo; xin.dong; dragos.axinte}@nottingham.ac.uk)

of the PKM. Whereas previous work focused on meeting these accuracy requirements without considering the locomotion capabilities, with studies on calibration [35] and path planning [25] tools for machining, we here present a complementary study that explores the influence of mechanism morphology on locomotion with both kinematic and stability models. This allows the intrinsic reconfigurability of the proposed design to be exploited to optimize both walking and machining performance in a wide range of conditions.

The development of a Reconfigurable Walking Machine Tool (RWMT) is here reported to address this challenge. The proposed design, presented in Section II, can adopt many forms, from symmetric to highly asymmetrical configurations, requiring a dedicated modeling framework for both kinematics and stability analysis, described in Section III. In Section IV, we study the capability of the proposed RWMT to improve speed, walking gait, and stability in a variety of terrain conditions. The proposed solution is proved to achieve safe operation in multiple environments with a reduced displacement error with the experiments in Section V.

II. A RECONFIGURABLE WALKING MACHINE TOOL

In this section, a novel concept of RWMT is proposed to enable complex path manipulation (e.g. for machining) together with the capability to adapt its configuration to intervention requirements. First, a general RWMT design is presented; we then focus on the reconfiguration mechanism on the moving platform, with six shape memory alloy (SMA) actuated clutches and a close-loop rope-pulley mechanism. Finally, four typical configurations of the proposed RWMT are introduced.

A. Conceptual design and challenges

As shown in Fig. 1, the proposed RWMT concept integrates a moving platform with a repositioning mechanism for the limbs. This represents a conversion of the conventional G-S platform by removing the fixed base (to “free” six feet) and adding reconfigurability to the connections on the mobile platform, as modelled in [35]. Specifically, the moving platform integrates a novel repositioning mechanism with six identical clutches on linear slides and a close-loop rope-pulley mechanism driven by a single motor (Fig. 1b). In each spherical-prismatic-spherical (SPS) limb, the upper S-joint is fixed to the clutch, which allows repositioning the limb layout on the moving platform (Fig. 1c). This is achieved by grasping the rope through the clutch, disengaging from the moving platform at the same time so that the upper S-joint can be dragged along the slider. When the clutch opens, the rope is released, and the S-joint fixes itself onto the moving platform. The moving platform is also designed to contain and protect the main electronics (2 FPGAs and 25 motor controllers).

When compared to conventional PKMs, the proposed RWMT provides not only the flexibility to adapt to the intervention site with free-positioning feet, but also an enhanced walking capability in challenging conditions, such as uneven surfaces and slopes. Walking is achieved by actively controlling the orientation of each limb with by driving the upper S-joints with a tendon-driven mechanism: in addition to the central linear motor of each limb (controlling limb length), three external motors are included to actuate tendons (Fig. 2c).

For a practical implementation of the proposed RWMT design, three main challenges need to be addressed:

- *Optimizing the layout of clutches on the moving platform.* In [25], a symmetric layout with each clutch positioned along the radial direction of the moving platform has been identified as optimal. By applying the Fourier-based methodology in [25], a new configuration can be obtained efficiently to avoid the singularities along a predefined machining path. However, the optimal layouts for locomotion have not been studied previously and are here addressed in Section III.
- *Switching the upper S-joints between passive and active modes.* A dual-mode tendon-driven upper S-joint [19], as shown in Fig. 2c, allows each upper S-joint to switch between passive and active modes by releasing and tensioning three tendons. The S-joint is in active mode when the tendons are tensioned and in passive mode when the tendons are released.
- *Positioning and actuating the clutches efficiently and compactly.* A lightweight repositioning clutch system is required, as conventional mechanisms are hindered by heavy and bulky designs with several motors and large transmission systems. Therefore, a novel repositioning system is essential for the proposed RWMT. Based on SMAs, the design of a smart actuation system is presented and discussed in the following subsection.

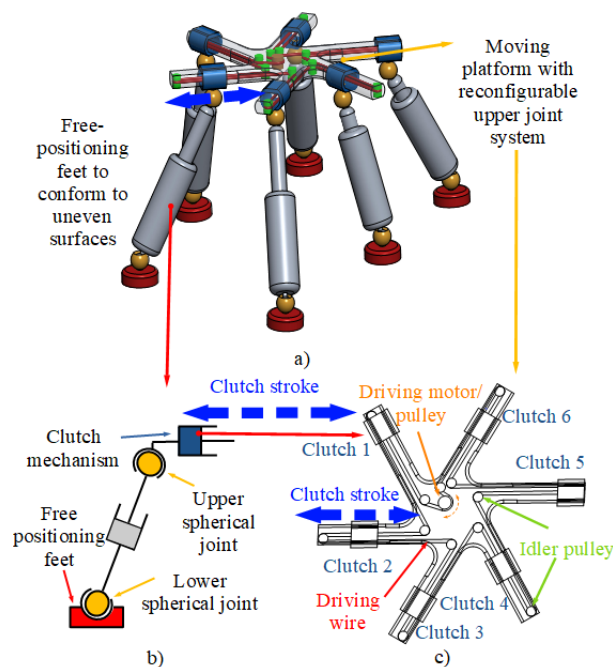


Fig. 1. Concept illustration of the proposed RWMT: a) Overview of the RWMT; b) Clutch-limb subsystem; c) Moving platform.

B. Smart Actuation System

SMAs are known for their capability to exert a high wrench compared to their volume [36]. This characteristic has allowed the creation of lightweight miniaturized systems incorporating SMAs in their design (when compared to electromechanical, hydraulic, and pneumatic actuators). Furthermore, successful applications of SMAs in the aerospace industry [37] and medical devices [38] have shown their advantages in metamorphic and intelligent structures as compact and

lightweight devices. For these reasons, SMAs have been selected for the development of a novel repositioning system. Aiming to reposition six clutches individually with a single motor, the novel Smart Actuation System (SAS) consists of six identical SMA based clutch mechanisms, six linear slides, a series of pulleys, a wire-rope band, and a single motor for its actuation, as shown in Fig. 2, where:

- Each SMA-clutch mechanism is integrated with a linear slide to position its upper S-joint along the radial direction (blue dashed arrow) of the moving platform.
- A wire-rope band (red component) passes through all the SMA-clutch mechanisms and moves in two directions (red dashed arrow).
- A series of idler pulleys (green components) guides the wire-rope band.
- A DC motor with a driving pulley (orange component) actuates the wire-rope band.
- A knot referencing mechanism is used to limit and reference the motion of the wire-rope band.

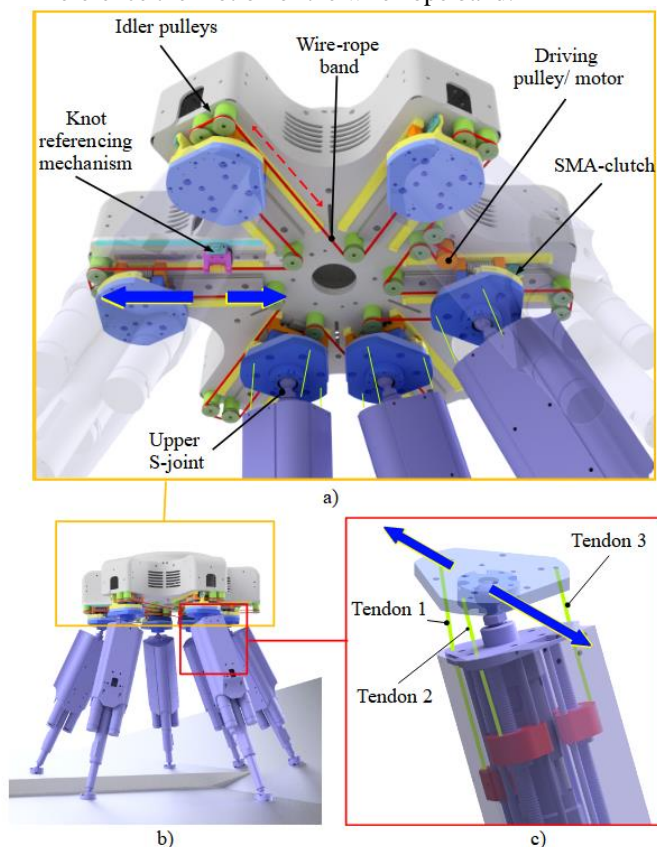


Fig. 2. Illustration of the proposed RWMT design: a) Detailed view of the SAS: a motor actuates a wire-rope band to reposition six upper S-joints; b) The RWMT over a scenario with uneven surfaces; c) Detailed view of the dual-mode tendon-driven upper S-joint.

The main advantage of the proposed SAS system is given by the SMA-clutches, which allow repositioning six limbs with a single motor that moves the wire-rope band: as the SMA-driven clutches can be opened or closed by applying current to the SMA wires, no additional motor is required. In contrast, conventional actuation packages would require a motor and its accessories (i.e. gearboxes, spindles, guides) for each limb. Thus, the smaller number of components needed for repositioning allows a lower moving platform mass, which is

critical for a good performance of the RWMT as the inertial forces during machining and walking are significantly reduced.

The novel design of the proposed SMA-clutch mechanism, as shown in Fig. 3a, is composed of a pair of shift pads, a pair of braking pads, an SMA wire, an encoder, and a linear guide. By heating or cooling the SMA wire with controlled voltage and current, the SMA-clutch mechanism grasps (Fig. 3c) and releases (Fig. 3b) the running wire-rope band while moving the shift pads to disengage (Fig. 3c) and engage (Fig. 3b) with the moving platform. The wire-rope passes through the center of each clutch and forms a closed loop on the moving platform. As such, the entire wire-rope band can be actuated by a single motor, as indicated in Fig. 2a, which can drive the six clutches either simultaneously or individually.

The SMA selection was based on stress, actuation force, applied current, and response time. Experimental test were performed to identify the optimal applied current to the SMA corresponding to the clutching force necessary to grasp the rope in less than 1s and move each limb with no slippage or failure. Therefore, by powering on/off the SMA wire and collaboratively actuating the wire-rope band, the proposed SMA-clutch mechanism can be utilized to displace one or more upper joints of the limb along with the slides.

As only a single motor is required for repositioning the six limbs simultaneously or individually, the load capacity of the wire-rope band needs to be significantly higher than conventional solutions (i.e. rubber bands with payload limit of 9 N) to actuate up to six clutches simultaneously. Thus, a steel-cored wire-rope cable is selected, with the wire-rope ends knotted together to form a loop. A knot referencing mechanism is implemented to track the knot position and prevent any blockage by the knot as shown in Fig. 3a.

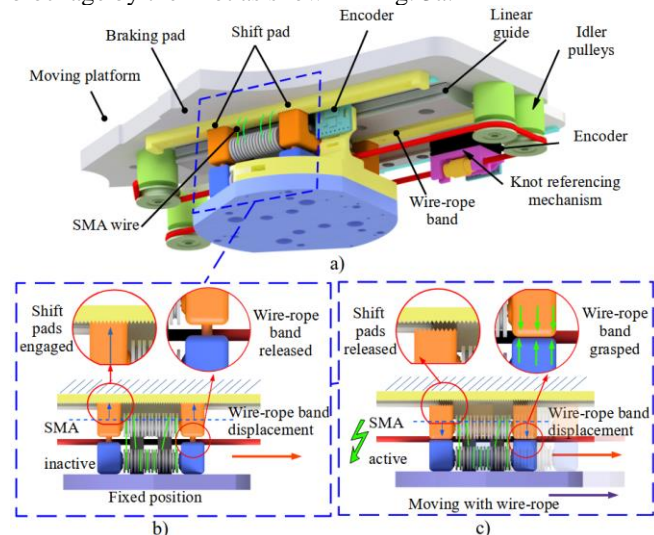


Fig. 3. Illustration of the SMA-clutch and working modes: a) Main components of the SMA-clutch; b) SMA inactive mode, the shift pads are engaged, and the position is locked; c) SMA active mode, the shift pads are disengaged, and the wire-rope band is grasped.

C. Configurations of Interest

The SAS can actuate the six upper joints simultaneously or individually, which allows optimizing the configuration of the proposed RWMT for different conditions (i.e. machining operations and walking on different terrains). This performance enhancement is due to various factors, such as singularity

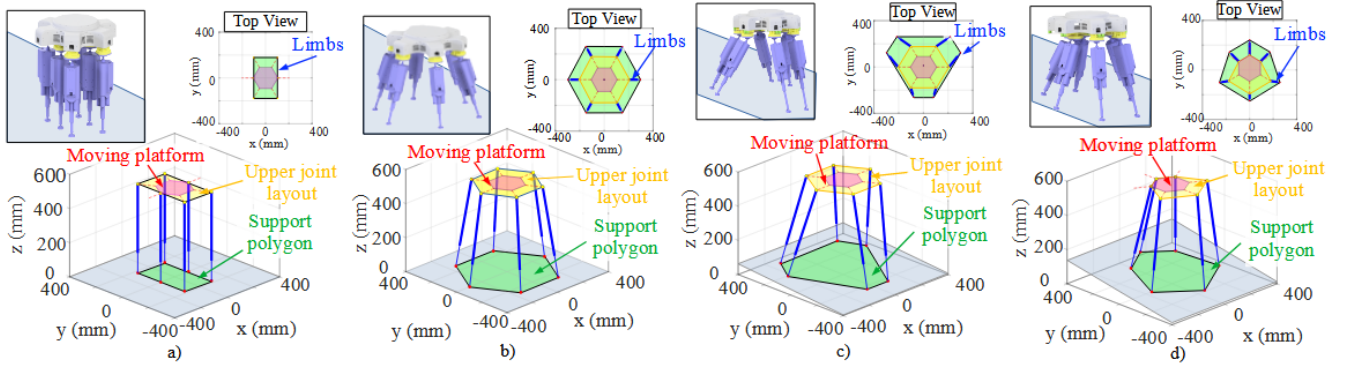


Fig. 4. Illustration of the proposed RPKWM with different configurations: a) Insect; b) Sym-Hex; c) G-S; d) Asy-Hex.

avoidance and optimized stiffness (when machining), and stability coefficient and gait speed when walking. Four configurations of interest are presented as follows:

- **Insect configuration** (Fig. 4a), with the upper joints aligned in two rows and limbs kept straight in the initial position. As the limbs maintain a quasi-vertical orientation, the feet can achieve the maximum height against the ground and thus avoid prominent obstacles with a rapid change in direction. Furthermore, as the limbs are lined up in two rows, the space required for walking is reduced, allowing the robot to navigate through narrow spaces.
- **Symmetrical Hexagonal configuration** (Sym-Hex, Fig. 4b), with a symmetric hexagonal layout of the upper joints with the six limbs evenly distributed around the centre of the moving platform. This configuration presents the biggest support polygon and highest stability coefficients. However, as the limbs operate close to their motion limit, the maximum stride in each step is reduced.
- **G-S configuration** (Fig. 4c), with the same layout of upper joints in the Sym-Hex configuration, but arranging the lower joints closer to each other in pairs. This configuration is well known in PKMs for its high accuracy and load capabilities [39]. Furthermore, compared with the Insect, it achieves higher stability with an increased support polygon.
- **Asymmetrical Hexagonal configuration** (Asy-Hex, Fig. 4d), with an asymmetric layout of upper joints. The uneven distribution of the six limbs around the centre of the moving platform allows a more efficient use of the workspace of each limb on inclined surfaces.

Thus, by reconfiguring the upper joints and removing the fixed base, two significant advantages are achieved, compared to conventional PKMs: the capability to adapt to the place of intervention and the ability to optimize configuration between walking and machining. Moreover, reconfigurability not only enhances stiffness and singularity avoidance, as presented in our previous work [25], but also improves stability and result in a better kinematic performance (e.g. higher speed, smaller displacement errors), as discussed in the following sections.

III. MODELLING AND GAIT ANALYSIS

This section presents the kinematic, stability and force analyses to determine the optimal configurations of the proposed RWMT for walking. First, a general kinematic model of the RWMT and its stability analysis are developed. Then, a force analysis for the tendons on the S-joints is reported. From

the results, a methodology to define optimal limb actuation is outlined to reduce motor forces by using different gaits and configurations. Finally, a comparison of the performance of different configurations for the RWMT is presented.

A. Coordinate systems

For the kinematics and stability analysis, a scheme of the proposed RWMT walking on a surface is shown in Fig. 5, where the following coordinate systems are defined:

- $\{O\}$ represents the global coordinate system, with the z -axis along the direction of gravity.
- $\{O_G\}$ represents the ground frame, where the x_G and y_G -axes lie on the plane defined by the ground surface. The x_G -axis is along the elevation gradient.
- $\{O_H\}$ represents the local frame fixed on the moving platform of the proposed RWMT, where O_H is at the centre of the moving platform. The x_H -axis points from O_H towards B_4 , and the y_H -axis points to the central location between B_5 and B_6 .
- $\{O_{B_i}\}$ represents the local coordinate system at the i^{th} upper joints, where O_{B_i} is located at the centre of the i^{th} upper S-joint (B_i), with the x_{B_i} -axis pointing towards O_H and z_{B_i} -axis parallel to z_H -axis; O_{B_i} is located on the $x_H y_H$ plane and the distance between O_{B_i} and O_H is defined as the motion parameter c_i and controlled by the SAS.

B. Kinematic and stability analysis

This analysis starts by defining the locations that describe the plane conforming the ground. For convenience, four border points of the ground are defined in $\{O_G\}$ by position vectors:

$${}^{O_G}\mathbf{G}_k = [x_j \ y_j \ z_j]^T \quad k = \{1, 2, \dots, 4\}. \quad (1)$$

Then, the position and orientation of the ground can be obtained in $\{O\}$ as:

$${}^O\mathbf{G}_k = {}^O\mathbf{R}_{O_G} {}^{O_G}\mathbf{G}_k + {}^O\mathbf{O}_G \quad (2)$$

where ${}^O\mathbf{R}_{O_G}$ is the rotational matrix from $\{O_G\}$ to $\{O\}$ and ${}^O\mathbf{O}_G$ is the position of O_G in $\{O\}$. The relative orientation of these two frames can be defined by a rotation of $\{O_G\}$ around the z axis and then a rotation around the y axis, which defines the ground inclination against the global frame. Moreover, three ground border point ${}^{O_G}_1$ to ${}^{O_G}_3$ are used to calculate a parametric equation of the ground plane as:

$$\mathbf{n} \cdot \mathbf{P}_{int} = \mathbf{n} \cdot \mathbf{P}_0 \quad (3)$$

where \mathbf{n} is a vector normal to the ground (obtained from ${}^{O_G}_1$ to ${}^{O_G}_3$), \mathbf{P}_{int} is a vector from O_G to the points of interest on the plane, and \mathbf{P}_0 is a vector pointing from O_G to a known

position on the ground. Then, to describe the origin of $\{O_H\}$, O_H is defined at $|H|$ from the ground (along the vector \mathbf{n} , see green line in Fig. 5). It can be noted that the distance c_i is controlled by the SAS clutch mechanism that is later used to reconfigure the RWMT. The position of each upper joint can be translated from $\{O_H\}$ to $\{O\}$ as:

$${}^0\mathbf{B}_i = {}^0\mathbf{R}_{O_H} {}^{O_H}\mathbf{B}_i + {}^0\mathbf{O}_H \quad (4)$$

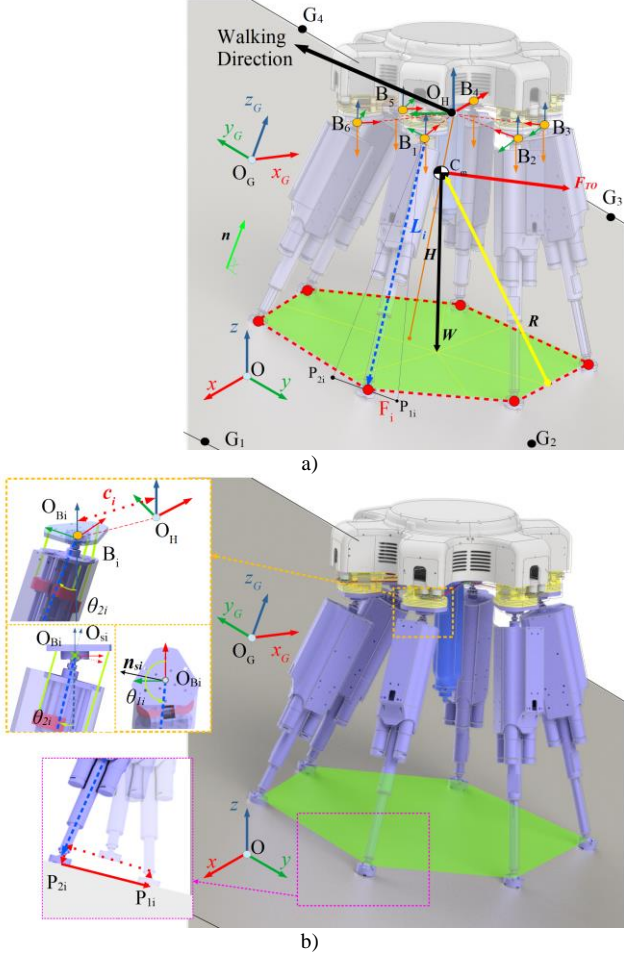


Fig. 5. Schematic of the RWMT on an inclined surface considering with kinematic parameters: a) General scheme; b) Component details.

Nevertheless, as different angles of roll, pitch and yaw are considered for the RWMT, the distance of the upper joints from the ground can be different, leading to complex interactions between the feet and the ground in inclined ground conditions. Thus, the feet should avoid collisions and remain at a constant distance from the ground during the swing stage in the walking operation. Referring to the detailed view of the i^{th} limb in Fig. 5b, further walking requirements are defined as follows:

- In the swing phase of the gait, the swing limbs must be lifted from the ground and swing in the direction and magnitude of the walking operation, maintaining a safe distance from the ground.
- In the support phase of the gait, all limbs must remain in contact with the ground and move backwards to produce the displacement of the platform.

The following procedure models ground-feet interaction:

Step 1. The neutral position of i^{th} limb from its upper joint B_i is defined to be parallel with z_H -axis and represented by a vector

$\mathbf{N}_{vi} \cdot \mathbf{P}_{vi}$ is the intersection point between \mathbf{N}_{vi} and the ground, which is written as:

$$\mathbf{P}_{vi} = {}^0\mathbf{B}_i + t_{vi}\mathbf{N}_{vi} \quad (5)$$

where t_{vi} is a coefficient defined by the intersection of \mathbf{N}_{vi} and the ground plane.

Step 2. The intersection between \mathbf{P}_{vi} and the ground plane is computed as a reference position for each limb. The intersection parameter t_{vi} can be obtained based on (3) and (5) as:

$$t_{vi} = (\mathbf{n} \cdot \mathbf{P}_0 - \mathbf{n} \cdot {}^0\mathbf{B}_i) / (\mathbf{n} \cdot \mathbf{N}_{vi}) \quad (6)$$

Step 3. \mathbf{P}_i is computed by (7) to define the starting location of i^{th} foot on the ground with respect to the neutral position. \mathbf{P}_i is defined at a distance A from \mathbf{P}_{vi} in the direction of the unit vector \mathbf{N}_{slide} ; A is a motion parameter related to the initial configuration of the RWMT and \mathbf{N}_{slide} is defined as the vector projection of the slides on the ground.

$$\mathbf{P}_i = \mathbf{P}_{vi} + A\mathbf{N}_{slide} \quad (7)$$

Step 4. To define gait motion, \mathbf{P}_{i1} and \mathbf{P}_{i2} are the forward (G_F) and backward (G_B) portions of a step vector along the walking direction \mathbf{W}_{dir} , defined for each foot as lying on the ground plane and parallel to the walking direction as:

$$\mathbf{P}_{i1} = \mathbf{P}_i + G_F\mathbf{W}_{dir} \quad (8)$$

$$\mathbf{P}_{i2} = \mathbf{P}_i - G_B\mathbf{W}_{dir} \quad (9)$$

Half-step gains G_F and G_B are here assumed as 0.5.

Step 5. The gait path is obtained as a sequence of points through an interpolation between \mathbf{P}_{i1} and \mathbf{P}_{i2} . To ensure stability in the walking process, the limbs in contact with the ground must create a support polygon that contains the projection of the center of mass (CoM) of the RWMT. The position of this projection is conventionally used to compute a static stability coefficient, defined as the smallest distance of the projection to an edge of the support polygon [33][42]. However, this criterion neglects the effect of the vertical position of the CoM, where a higher position will diminish the stability. Therefore, this paper supplements the static stability coefficient with an evaluation of the force required to tip over the RWMT (\mathbf{F}_{T0}) as expressed by:

$$\sum \mathbf{M}_a = (\mathbf{R} \times \mathbf{W}) + (\mathbf{R} \times \mathbf{F}_{T0}) = 0, \quad (10)$$

where \mathbf{R} is the smallest distance vector from the edge of the support polygon to the CoM, \mathbf{W} is the weight of the RWMT, and \mathbf{F}_{T0} is the necessary force to maintain static equilibrium and prevent the rotation of the robot around the edge of the support polygon (considering the shortest distance from the projection of the CoM). Then, \mathbf{F}_{T0} is normalized against the weight of the robot. This index is positive for stable conditions, and as its value approaches zero the system becomes less stable; if the index becomes negative the system is unstable. More importantly, this criterion allows a full evaluation of the stability of the RWMT in different configurations over diverse conditions for the ground (i.e., inclined ground), whereas the static stability coefficient is optimized for flat surfaces only.

C. Limb actuation analysis

The limb design and actuation are based on the 3-DoF mechanism concept presented in [43]. However, to understand the influence of different configurations over the key components in the proposed RWMT, a FEA model is created in ANSYS APDL[®]. Based on this model, the moments required to actuate the upper S-joints and the reaction forces between the feet and ground can be obtained during different stages in the walking process, which is divided into a finite number of sub-

steps. In this way, a full walking cycle can be characterized to select the most feasible configurations for walking in terms of the forces exerted on the components. To reduce the computational burden, the FEA model is defined as follows:

- The limbs are considered to perform as beam elements.
- The upper joints are rigidly connected to the platform.
- Lumped masses in the CoM of each component.
- The linear displacement of supporting feet is constrained.

The reaction forces and moments obtained from the FEA model are later used to evaluate the tensile forces on the tendons actuating each limb. As the tendons are the most critical component in the limbs, this procedure is needed to prevent excessive loading and operation failure. For this reason, a static model of the limbs is implemented by considering the moments supported by the tendons, the moments created by the weight of each limb, and the reaction forces of the feet with respect to the center of the joints, based on the results of the FEA model. The equations describing the equilibrium of each joint is:

$$\sum_{j=1}^3 \mathbf{F}_{ij}(\mathbf{r}_{ij} \times \mathbf{D}_{ij}) + m_l(\mathbf{r}_w \times \mathbf{g}) + (\mathbf{r}_{fi} \times \mathbf{R}_{fi}) = \mathbf{0} \quad (11)$$

where \mathbf{F}_{ij} is the force exerted by j^{th} tendon in the i^{th} limb, \mathbf{r}_{ij} is a vector from the centre of the i^{th} spherical joint to the j^{th} lower tendon guide, \mathbf{D}_{ij} is the vector representing the direction of the j^{th} tendon (as a unit vector) in the i^{th} limb, m_l is the mass of each limb, \mathbf{r}_w represents the radius of action of the limb's mass, \mathbf{g} is the acceleration produced by the gravity, \mathbf{r}_{fi} is the radius of action of the reaction force of the i^{th} foot, and \mathbf{R}_{fi} is the reaction force on the i^{th} foot. By solving (11), the forces exerted in the tendons can be computed to evaluate tendon forces in different configurations and select the optimal RWMT gaits.

D. Walking performance analysis

As the proposed RWMT can modify its upper joint configuration, different layouts can be arranged to increase the performance of the RWMT over different walking conditions, such as low friction surfaces, slopes, obstacles. As presented in Section II-C, four configurations are considered in this paper: Insect, Sym-Hex, G-S and Asy-Hex. These configurations are compared under different terrain conditions (flat and inclined ground at 4° and 10°) with two typical gaits (wave and tripod).

We here analyze how performance can be optimized through two parameters: gait speed (related to the maximum step length) and actuation forces (as tendon tension). As the robot performs differently when walking on flat or inclined ground, these two environments are discussed separately, and an additional stability analysis is presented for the inclined surface scenario.

The maximum step length of the robot is influenced by the height of the top platform from the ground; the physical motion limits of each actuator and components of the RWMT; the need to avoid internal and external collisions; and the stability of the system. Larger obstacles on the ground can be avoided with higher platform configurations. However, this affects the stability of the system as reported in Fig. 6, which shows the maximum step lengths achieved by each configuration as a function of the selected platform height and summarizes the equilibrium condition limiting the maximum step size for the Insect and Sym-Hex configurations.

A lower but consistent maximum step length can be observed in the Insect configuration, whereas the maximum step length is significantly reduced in the Sym-Hex configuration for any height greater than 565mm. This pattern allows the Insect configuration to perform a stable walking with similar gait characteristics (e.g., step height and length) independently of the required platform height, as it can be adjusted according to the environment without a significant impact on performance.

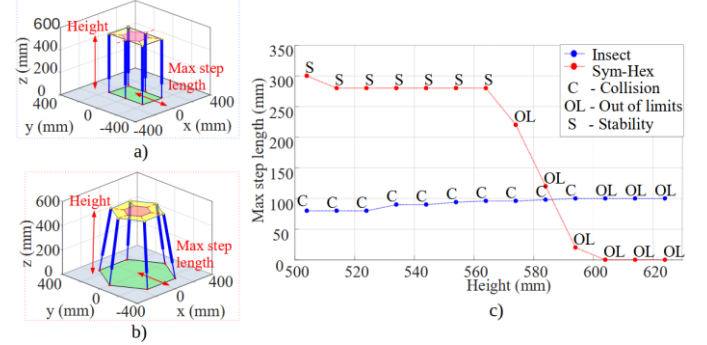


Fig. 6. Maximum step length comparison: a) Insect; b) Sym-Hex and c) Maximum step length vs platform height.

1) Flat ground

For the flat ground scenario, the Insect and Sym-Hex configurations are selected, and the tendon forces are evaluated for the tripod and wave gaits. In the tripod gait the limbs are actuated in two groups, which cycle between support and swinging in the air with a cooperative mode; in the wave gait, each limb is repositioned individually while the rest maintain contact with the ground to later effectuate the displacement of the RWMT. In both cases, the maximum tendon loads are evaluated to prevent situations that could induce damage to the components, as high forces will induce larger deformations on the tendons and deviate the limbs from their ideal position. Moreover, both the Insect and Sym-Hex configurations are evaluated, and the results are summarized in Fig. 7, which presents the maximum tensile forces exerted on the tendons of each joint and the difference between the wave and tripod gaits. The gait comparison, based on Section III-C and shown in Fig. 7c and Fig. 7f, is expressed as:

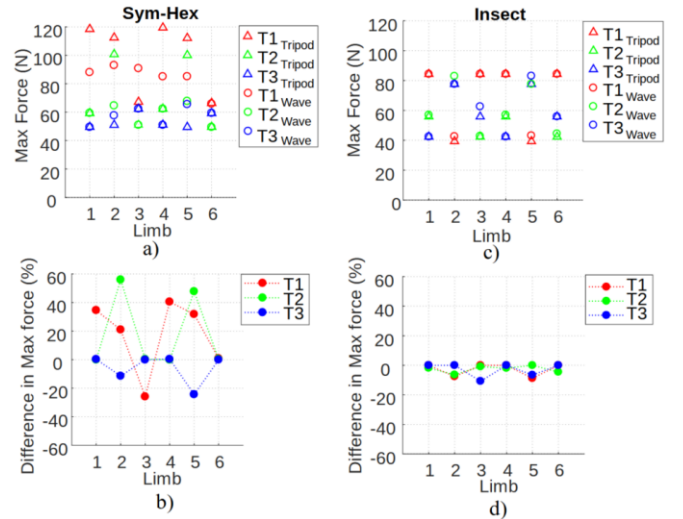


Fig. 7. Force analysis for the tendons: a) Tripod and wave gait max force for Sym-Hex; b) Difference between gaits for Sym-Hex; c) Tripod and wave gait max force for Insect; d) Difference between gaits for Insect.

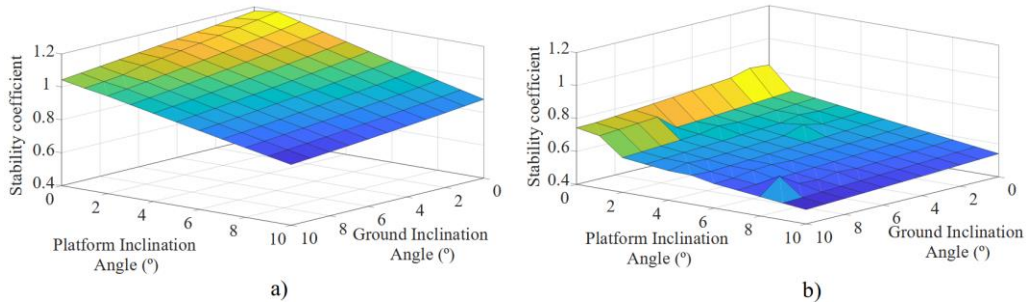


Fig. 8. Case study for the optimal attitude of the RWMT. Variation of the stability coefficients considering different platform pitch and ground inclinations. a) G-S configuration; b) Sym-Hex configuration.

$$T_{ij\%} = \left(\frac{T_{Tij} - T_{Wij}}{T_{Wij}} \right) \times 100 \quad (12)$$

where T_{Tij} and T_{Wij} represent the maximum tensile force on the j^{th} tendon for the i^{th} limb with the tripod and wave gaits, respectively. As per Fig. 7a, the most significant variation in forces occurs with the Sym-Hex configuration and the tripod gait, which represents an increment of up to 60% of the tendon tension force compared with the wave gait (Limb 2-T2). The maximum force found in the tendons for the Sym-Hex configuration is reduced from 119.5 N to 80 N, with the wave gait (Limb 4-T1) representing a difference of 40%. For these reasons, the wave gait is selected for the Hexagonal (symmetric and asymmetric) and G-S configurations. However, for the Insect configuration, the maximum forces exerted on the tendons are similar in both tripod and wave gait. In the Insect configuration the wave and tripod gaits can be used without significantly modifying the load conditions on the critical components of the RWMT. However, the time required to perform each displacement of the moving platform is smaller with the tripod gait. For this reason, the tripod gait is selected for the Insect configuration.

2) Inclined ground

Traversing over inclined ground affects the stability of an RWMT and configurations with increased stability must be considered. As such, this section presents a study of the effects of traversing over inclined surfaces with different configurations. First, we compare the Insect, Sym-Hex, and G-S configurations considering different slope angles and keeping the moving platform parallel to the (inclined) ground. Then, the effect of traversing inclined ground with different pitch angles (i.e. relative angles between the moving platform and the inclined ground) is discussed.

The behavior of the Insect, Sym-Hex, and G-S configurations on a 0° to 10° ground inclination (i.e., the angle between the x_g -axis and the xy plane) is reported in Fig. 8 for the moving platform parallel to the ground, constraining the normal vector of the ground \mathbf{n} to be parallel to the z_H -axis. The results show the stability coefficient of the Insect configuration as stable and close to constant. Conversely, G-S and Sym-Hex have higher stability coefficients (up to three times) but decrease with inclination. Overall, the reduced stability coefficient of the Insect configuration could lead to damage to the RWMT. For these reasons, the rest of this section focuses on the G-S and Hexagonal configurations only over inclined surfaces.

We then analyze the effect of the relative angle between the pitch angle (defined as the angle formed between the z_H -axis and the xy plane) of the RWMT and the ground angle over the

stability coefficients, as changing this angle between \mathbf{n} and the z_H -axis of the RWMT affects the relative location of the CoM against the support polygon. For this study, we consider grounds with inclinations from 0° to 10° (i.e., angle between \mathbf{n} and XY plane). Similarly, the pitch angle of the RWMT (i.e. angle between \mathbf{n} and z_H -axis) ranges between 0° and 10° . By studying the relative angle between the platform and the ground inclination, the best configuration can be chosen to traverse different terrains. As already observed in Fig. 8, the results in Fig. 9 show that increasing ground inclination while maintaining the platform parallel to the ground (i.e., the angles between the RWMT platform and the ground increase evenly) negatively affects stability. Negative angles also decrease stability coefficients and reduce the usable workspace of each limb (see Fig. 10), which is at its maximum when the moving platform is parallel to the ground (i.e. when z_H and z_G are parallel). The maximum stability coefficients are obtained at a platform pitch of 0° , when the z_H - and z -axes are parallel. These results consider the locations of the upper joints to be symmetrical in the G-S and Sym-Hex configurations, with all the joints on the upper platform at the same radial distance from O_H . However, these configurations are not optimal for the workspace, which increases for diverging z_H - and z_G -axes.

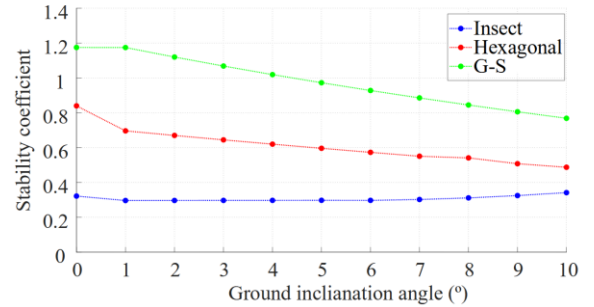


Fig. 9. Stability coefficients between 0° and 10° of inclination for the ground inclination (the platform is considered parallel to the inclined surface).

Further limitations are observed at high inclinations:

- The frontal limbs operate at the top of the workspace of each limb, restricting the minimum limb length (Fig. 10, red rectangle).
- The rear limbs operate at the bottom of the workspace of each limb, restricting the maximum limb length (Fig. 10, yellow rectangle).

These constraints would limit conventional PKMs to operate in Hexagonal and G-S configurations even at lower slope angles. However, as the upper joints are repositionable, the joints on the moving platform can be configured

asymmetrically (Asy-Hex) to increase the maximum ground inclination that the RWMT can traverse.

Overall, in this section the performance of a new concept of RWMT has been evaluated based on an efficient methodology for the kinematic, stability and force analyses. These models enable a numerical quantification of the RWMT performance considering the reconfiguration capabilities and different terrain conditions. Furthermore, the result show that the RWMT can enhance its performance in terms of stability, walking gaits, forces exerted on the critical components and a better use of the workspace of each limb, by making use of its reconfigurable capabilities, as shown in Fig. 11. These results are validated in the next section in a set of experiments with a RWMT prototype walking in different terrain conditions.

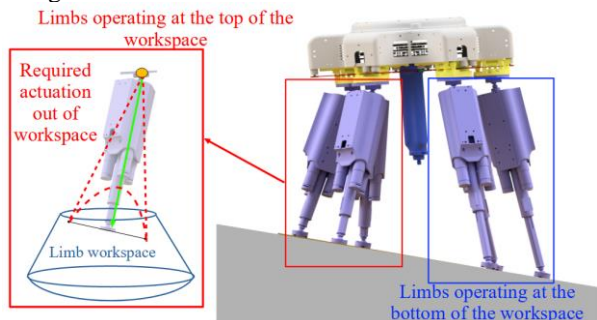


Fig. 10. Illustration of the RWMT operating at a highly inclined surface. The frontal limbs work at the top of the workspace, while the rear limbs operate at the bottom of the workspace, limiting the displacement of the RWMT.

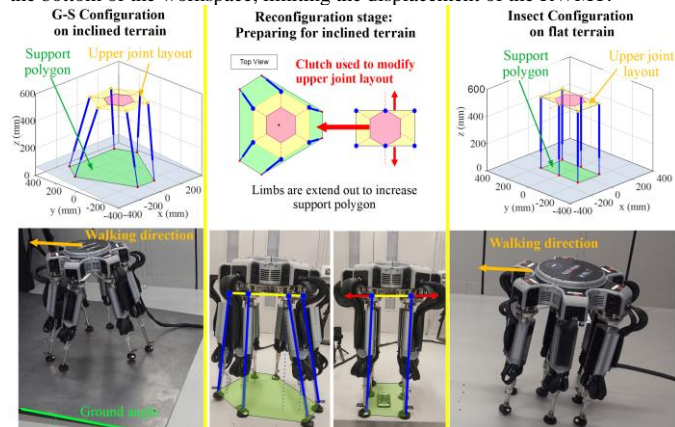


Fig. 11. The proposed RWMT enhancing its stability from flat to inclined terrain by increasing its support polygon, reconfiguring the position of the upper joints and lower joints to safely walk over inclined terrain.

IV. EXPERIMENTAL TESTS AND RESULTS

In this section, to validate the modeling and gait analysis in Section III, a prototype of the proposed RWMT has been built and tested. A VICON® motion capture system with four Vantage cameras was used to measure the movement of the RWMT. Three and five reflective markers have been added to the upper platform and to each lower joint, respectively, in order to track the poses of feet and upper platform for the evaluation of the walking performance.

First, the Insect and Sym-Hex configurations have been tested with tripod and wave gaits. These configurations with their ideal displacements have been compared against the motion recorded by the tracking system. Then, the G-S and the Sym-Hex configurations have been compared in displacement on an inclined terrain at 4°. Finally, non-symmetrical layouts of

the G-S and Hexagonal configurations are reported for traversing an inclined terrain at 10°, to highlight the adaptability characteristics of RWMT in traversing different terrains.

A. Gait selection for the different configurations

The first comparison tests the tripod and wave gaits for the Insect and Sym-Hex configurations. When testing the proposed gaits (tripod and wave), the Sym-Hex configuration fails in the tripod gait, as the load on the tendons increases critically when three limbs are lifted from the ground (as shown in Section III-D1.), resulting in a significant motion error. However, the wave gait has been successfully implemented in the Sym-Hex configuration. Conversely, the Insect configuration can achieve tripod and wave gaits as the forces on the tendons are reduced compared to the Sym-Hex (shown in Section III-D1). This shows not only a more stable tendon load pattern, but also means that a longer operational life can be expected from the tendons actuating each joint, further preventing a possible failure during its walking operations.

Once selected the appropriated gaits for each configuration, the capability to traverse over different terrains has been evaluated. Three test terrains are here proposed: flat ground and inclined grounds at 4° and 10°.

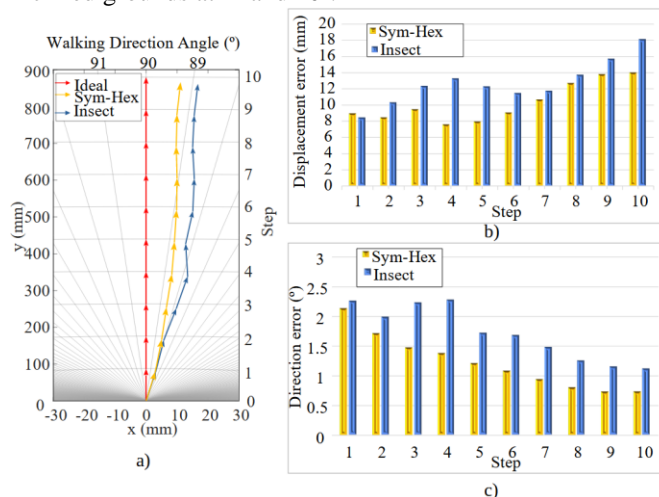


Fig. 12. Comparison between the Sym-Hex and Insect configurations: a) Displacements of the Sym-Hex and G-S configuration against the ideal displacement; b) Displacement error; c) Direction error.

B. Flat ground

The Insect and Sym-Hex configurations are here proposed to test the motion capabilities of the proposed RWMT, evaluated as the time required to traverse the same distance (i.e. the average speed of the configuration) and the comparison between the desired motion and the real one. Fig. 12 presents the results obtained during the walking of both configurations at the different stages. As both configurations aim at a total displacement of 880 mm, each step is characterized by a ground displacement of 88 mm, as highlighted with arrows in Fig. 12a. Furthermore, the error of the displacements and deviation were evaluated at the end of each step.

Fig. 12b-c present the displacement error, defined as the error between the desired and real magnitude of displacement, and the direction error, defined as the error between the desired and real displacement direction, for both configurations. The results show both the error on each step and how these errors

accumulate as the RWMT keeps moving. In both configurations, the maximum deviation error is observed at the beginning, and the error value decreases at each step. The Insect configuration has the highest error at each step. Nevertheless, the maximum difference between both configuration in the displacement errors of each configuration is smaller 5.72 mm and 1.14°. Furthermore, the Insect configuration completes a gait cycle every 1.60 minutes, while the Sym-Hex performs a gait cycle every 2.94 minutes. Thus, the Insect configuration moves 1.8 times faster than the Sym-Hex configuration.

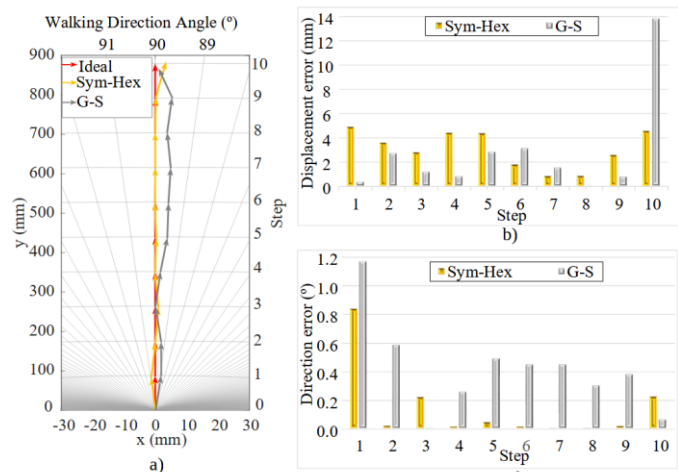


Fig. 13. Comparison between the Sym-Hex and G-S configurations: a) Displacements of the Sym-Hex and G-S configuration against the ideal displacement; b) Displacement error; c) Angular displacement error.

C. Inclined ground at 4°

The Sym-Hex and G-S configurations are here selected for their increased stability coefficients when compared to the Insect configuration. The required displacement is again equal to 880 mm in 10 steps, this time performed on an inclined terrain at 4°. As shown in Fig. 13b-c, the maximum error is observed in the first step of the Sym-Hex configuration in both traversed distance and deviation error. Similarly, the G-S presents the maximum direction error during the first step, but the maximum displacement error occurs during the last step. The deviation angles of the G-S configuration are significantly higher than those of Sym-Hex, indicating a more erratic pattern.

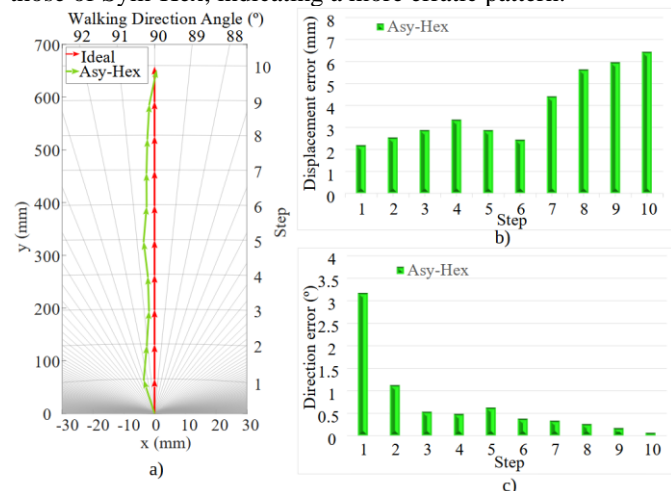


Fig. 14. Asy-Hex configuration: a) Comparison of ideal and real displacement; b) Displacement errors at each step; c) Direction errors at each step.

D. Inclined ground at 10°

The Sym-Hex and G-S configurations are here selected for their increased stability coefficients when compared with the Insect configuration. However, when the ground inclination is increased, the usable workspace of each limb is reduced, as mentioned in Section III-D2, and we propose non-symmetrical configurations to achieve stable displacements: the upper S-joints of the frontal limbs are brought closer to the center of the platform, while the ones in the rear limbs are brought to the end of the slides. The required displacement in this test is 660 mm in 10 steps, performed on an inclined ground at 10°. When the G-S configuration is tested, a considerable slippage is observed, and this configuration is thus discarded.

Conversely, the Asy-Hex configuration is capable of moving on inclined ground at 10°, with the results reported in Fig. 14. The Asy-Hex configuration shows its maximum displacement error at the last step and a total error of 6.42 mm. As observed in the previous tests, the maximum direction error occurs at the first step and decreases in subsequent steps.

Overall, the proposed RWMT has been successful in modifying its configuration to stably walk in conditions that would limit conventional parallel kinematic walking machines.

V. DISCUSSION OF RESULTS

In the previous section, Fig. 12 presented a comparison between the Insect and Sym-Hex configurations on flat ground; a higher direction error can be observed for the Insect configuration. However, the overall motion presents no significant deviation from the desired one in both configurations (smaller than 5 mm, over a total gait length of 880 mm). Furthermore, in Fig. 8b and Table I, a reduced stability coefficient can be observed in the Insect configuration when compared to the Hexagonal configurations, indicating that the reduced stability coefficient might cause the slightly larger error observed. However, the maximum deviation error is within 2°, and the Insect configuration has an advantage in its higher speed (1.8 times faster than the Sym-Hex). More importantly, the direction error over long distances can be solved as the Insect configuration can move laterally, as the Insect configuration enables changes in the walking direction of 90° with no required turning angle. Furthermore, the test also shows that the Insect configuration can avoid obstacles in the path of the RWMT (video in the supplementary material).

The relationship between stability coefficient, the configuration symmetry and displacement error can also be observed when the G-S and the Sym-Hex configurations are compared on an inclined ground at 4°. The Sym-Hex configuration presented a better performance in terms of direction error over the full trajectory, as reported in Fig. 13c, and a maximal displacement error of 4.9 mm. Thus, the Sym-Hex configuration is the most suited for traversing an inclined ground, showing that more symmetrical configurations present a better performance in achieved displacement. When non-symmetrical G-S and Hexagonal configurations are compared at higher angles, slippage is seen in the G-S configuration, making it non-suitable for traversing an inclined ground at 10°.

Regarding Hexagonal configurations, the symmetrical configuration shows a better performance at low inclination angles, while steeper slopes require non-symmetrical

configurations for safety and to operate within the mechanical limits of the design.

In conclusion, three configurations of the RWMT are proposed to traverse different terrain conditions optimally:

- *Insect configuration*: Proposed to move on flat ground when the main concerns are speed and obstacle avoidance.
- *Symmetric Hexagonal*: Proposed to move on inclined grounds when the limbs operate within allowable limits.
- *Non-Symmetric Hexagonal*: Proposed to move on highly inclined ground when the limbs are required to operate at their maximum actuation limits.

TABLE I
PERFORMANCE COMPARISON

Configuration	Insect	Sym-Hex	GS	Asy-Hex.	
Ground inclination (°)	0	0	4	10	
Max error (mm)	18.2	10.1	4.9	13.9	6.4
Max direction error (°)	9.6	2.4	0.8	1.2	3.2
Average error (mm)	12.8	10.2	3	2.7	3.8
Min stability coefficient	0.3	0.9	0.9	1.1	0.8
Speed (step/min)	0.6	0.3	0.3	0.3	0.3

VI. CONCLUSIONS

This paper proposes the concept and design of a new Reconfigurable Walking Machine Tool (RWMT), which can modify its configuration from symmetric to irregular layouts by repositioning its joints. This metamorphism allows the novel RWMT to adapt to different terrains where conventional PKM can neither walk nor operate, while maintaining high-precision machining capabilities, comparable to the ones of a conventional workshop machine tool, after reconfiguration. When compared to other mobile robots, the proposed RWMT is lightweight and compact thanks to its parallel architecture, employed for both machining and walking rather than requiring two separate subsystems for locomotion and operation, and to its underactuated reconfiguration mechanism, with a single motor to operate multiple DoFs. The main contributions of this paper can be summarized in the following points:

- *Design of a novel RWMT*: The concept of reconfigurable Gough-Stewart platform has been introduced in previous works, but this paper presents for the first time a complete design solution to achieve full reconfigurability by combining active/passive spherical joints, the novel SMA-driven clutch design, and the underactuated rope-driven upper platform layout.
- *Analysis of walking capabilities*: Locomotion performance has been characterized with kinematic and static modelling and a stability analysis of different configurations, to identify the optimal layout for each scenario.
- *Experimental validation*: The RWMT locomotion has been tested on inclined and flat terrain, comparing the performance of four different configurations (i.e. Sym-Hex, Insect, Gough-Stewart and Asy-Hex) at increasing slope angles. The best configuration for each scenario has been identified, prioritizing speed at lower slopes and stability at higher inclinations.

The models and methods presented in this paper open the opportunity for the development of other portable machine tools capable of reconfiguration. In future works, further configurations and layouts can be explored, expanding the

proposed design to other applications (e.g. manipulation) and different mechanism architectures.

VII. REFERENCES

- [1] P. Gonzalez de Santos, J. Estremera, and E. Garcia, "Optimizing leg distribution around the body in walking robots," *Proceedings of the 2005 IEEE International Conference on Robotics and Automation*, pp. 3207-3212, 2005.
- [2] B. Li, Y. Li, J. Ruan X Rong, "Research of mammal bionic quadruped robots a review," *IEEE 5th International Conference on Robotics, Automation and Mechatronics* pp. 166-171, 2011.
- [3] J.-P. Merlet, *Parallel Robots*, Second ed. ed. Springer, 2006.
- [4] M. Ceccarelli, M. Russo, and C. Morales-Cruz, "Parallel architectures for humanoid robots," *Robotics* vol. 9, no. 4, pp. 75, 2020.
- [5] Z. Wang, W. Delun, S. Yu, X. Li, and H. Dong, "A reconfigurable mechanism model for error identification in the double ball bar tests of machine tools," *International Journal of Machine Tools and Manufacture*, vol. 165, pp. 103737, 2021.
- [6] J. L. Olazagoitia and S. Wyatt, "New PKM Tricept T9000 and its application to flexible manufacturing at aerospace industry," *SAE Technical Papers*, vol. 1, 2007.
- [7] S. N. Yurt, I. B. Özkol, M. O. Kaya, and C. Hacıyev, "Optimization of the PD coefficient in a flight simulator control via genetic algorithms," *Aircraft Engineering and Aerospace Technology*, vol. 74, no. 2, pp. 147-153, 2002.
- [8] C. Li, H. Wu, H. Eskelinen, H. Handroos, and M. Li, "Design and implementation of a mobile parallel robot for assembling and machining the fusion reactor vacuum vessel," *Fusion Engineering and Design* vol. 161, pp. 111966, 2020.
- [9] Z. Liao, Q.H. Wang, H. Xie, J. Li, X. Zhou, and P. Hua, "Optimization of robot posture and workpiece setup in robotic milling with stiffness threshold," *IEEE/ASME Transactions on Mechatronics*, 2021.
- [10] Z. Xie, F. Xie, X.J. Liu, J. Wang, and B. Mei, "Tracking error prediction informed motion control of a parallel machine tool for high-performance machining," *International Journal of Machine Tools and Manufacture*, vol. 164, pp. 103714, 2021.
- [11] X. Yang, L. Zhu, Y. Ni, H. Liu, W. Zhu, H. Shi, and T. Huang, "Modified robust dynamic control for a diamond parallel robot," *IEEE/ASME Transactions on Mechatronics* 24, no. 3, pp. 959-968, 2019.
- [12] K. Wen, and C. Gosselin, "Static Model Based Grasping Force Control of Parallel Grasping Robots with Partial Cartesian Force Measurement," *IEEE/ASME Transactions on Mechatronics*, 2021.
- [13] Z. Chen, F. Gao., "Time-optimal trajectory planning method for six-legged robots under actuator constraints," *Proceedings of the Institution of Mechanical Engineers, Part C: Journal of Mechanical Engineering Science*, vol. 233, no. 14, pp. 4990-5002, 2019.
- [14] M. Ceccarelli, D. Cafolla, M. Russo, and G. Carbone, "HeritageBot platform for service in Cultural Heritage frames," *International Journal of Advanced Robotic Systems* 15, no. 4 (2018): 1729881418790692.
- [15] M. Russo, D. Cafolla, and M. Ceccarelli, "Design and experiments of a novel humanoid robot with parallel architectures," *Robotics* vol. 7, no. 4 pp. 79, 2018.
- [16] S. Kumar et al. "Kinematic analysis of a novel parallel 2SPRR+ 1U ankle mechanism in humanoid robot." In *International Symposium on Advances in Robot Kinematics*, pp. 431-439. Springer, Cham, 2018.
- [17] Y. Tian, F. Gao, "Efficient motion generation for a six-legged robot walking on irregular terrain via integrated foothold selection and optimization-based whole-body planning," *Robotica* vol. 36, no. 3, pp. 333-352, 2018.
- [18] D. Feller and S. Christian, "Mechanical design and analysis of a novel three-legged, compact, lightweight, omnidirectional, serial-parallel robot with compliant agile legs," *Robotics* vol. 11, no. 2, pp. 39, 2022.
- [19] J. Sun and J. Zhao, "An adaptive walking robot with reconfigurable mechanisms using shape morphing joints," *IEEE Robotics and Automation Letters*, vol. 4, no. 2, pp. 724-731, 2019.
- [20] H. Zhang, "Mechanics Analysis of Functional Origamis Applicable in Biomedical Robots," *IEEE/ASME Transactions on Mechatronics*, 2021.

- [21] E. Romiti et al. "Toward a Plug-and-Work Reconfigurable Cobot," *IEEE/ASME Transactions on Mechatronics*, 2021.
- [22] A. Fomin, A. Antonov, V. Glazunov, and G. Carbone. "Dimensional (parametric) synthesis of the hexapod-type parallel mechanism with reconfigurable design." *Machines* vol. 9, no. 6, pp. 117, 2021.
- [23] E. Donato, G. Picardi, and M. Calisti. "Statics Optimization of a Hexapedal Robot Modelled as a Stewart Platform." In *Annual Conference Towards Autonomous Robotic Systems*, pp. 370-380. Springer, 2021.
- [24] M. Russo, N. Sriratanasak, W. Ba, X. Dong, A. Mohammad and D. Axinte, "Cooperative Continuum Robots: Enhancing Individual Continuum Arms by Reconfiguring Into a Parallel Manipulator," in *IEEE Robotics and Automation Letters*, vol. 7, no. 2, pp. 1558-1565, 2022.
- [25] J. Camacho, M. Wang, X. Dong, and D. Axinte, "A novel class of rpkm concepts and Fourier-base singularity analysis" *Mechanism and Machine Theory*, vol. 153, 2020.
- [26] P. Gonzalez de Santos, E. Garcia, and J. Estremera, "Improving walking-robot performances by optimizing leg distribution," *Autonomous Robots*, vol. 23, no. 4, pp. 247-258, 2007.
- [27] K. Ozyalcin, I.H. Akay, Y. Ozturk, B. Mengus, H. Ozakyol and Z. Bingul, "New design and development of reconfigurable hybrid hexapod robot," *Annual Conference of the IEEE Industrial Electronics Society*, pp. 2583-2588, 2018.
- [28] G. Zhong, L. Chen, and H. Deng, "A performance oriented novel design of hexapod robots," *IEEE/ASME Transactions on Mechatronics*, vol. 22, no. 3, pp. 1435-1443, 2017.
- [29] H. Yang, S. Krut, C. Baradat, and F. Pierrot, "Locomotion approach of REMORA: A reconfigurable mobile robot for manufacturing Applications," *International Conference on Intelligent Robots and Systems*, pp. 5067-5072, 2011.
- [30] N. Plitea, D. Lese, D. Pislea, and C. Vaida, "Structural design and kinematics of a new parallel reconfigurable robot," *Robotics and Computer-Integrated Manufacturing*, vol. 29, no. 1, pp. 219-235, 2013.
- [31] K. S. Yang H., and Pierrot, F., "A new concept of self-reconfigurable mobile machining centers," *IEEE/RSJ International Conference on Intelligent Robots and Systems*, pp. 2784-2791, 2010.
- [32] D. Axinte et al., "MiRoR—Miniaturized robotic systems for holistic in-situ repair and maintenance works in restrained and hazardous environments," *IEEE/ASME Transactions on Mechatronics*, vol. 23, no. 2, pp. 978-981, 2018.
- [33] A. Rushworth, S. Cobos-Guzman, D. Axinte, and M. Raffles, "Pre-gait analysis using optimal parameters for a walking machine tool based on a free-leg hexapod structure," *Robotics and Autonomous Systems*, vol. 70, pp. 36-51, 2015.
- [34] A. Olarra, D. Axinte, L. Uriarte, and R. Bueno, "Machining with the WalkingHex: A walking parallel kinematic machine tool for in situ operations," *CIRP Annals*, vol. 66, no. 1, pp. 361-364, 2017.
- [35] M. Russo and X. Dong, "A calibration procedure for reconfigurable Gough-Stewart manipulators," *Mechanism and Machine Theory*, vol. 152, p. 103920, 2020.
- [36] P. Motzki, F. Khelfa, L. Zimmer, M. Schmidt, and S. Seelecke, "Design and validation of a reconfigurable robotic end-effector based on Shape Memory Alloys," *IEEE/ASME Transactions on Mechatronics*, vol. 24, no. 1, pp. 293-303, 2019.
- [37] D. Hartl, B. Volk, D. C. Lagoudas, F. Calkins, and J. Mabe, "Thermomechanical characterization and modeling of Ni60Ti40 SMA for actuated chevrons," *ASME international mechanical engineering congress and exposition*, pp. 281-290, 2006.
- [38] N. Jang et al., "Compact and lightweight end-effectors to drive hand-operated surgical instruments for robot-assisted microsurgery," *IEEE/ASME Transactions on Mechatronics*, vol. 25, no. 4, pp. 1933-1943, 2020.
- [39] C. Yuan, R. Gexue, and D. ShiLiang, "Vibration control of Gough-Stewart platform on flexible suspension," *IEEE Transactions on Robotics and Automation*, vol. 19, no. 3, pp. 489-493, 2003.
- [40] M. Wittlinger, R. Wehner, and H. Wolf, "The desert ant odometer: a stride integrator that accounts for stride length and walking speed," *J Exp Biol*, vol. 210, no. Pt 2, pp. 198-207, Jan 2007.
- [41] M. Grabowska, E. Godlewska, J. Schmidt, and S. Daun-Gruhn, "Quadrupedal gaits in hexapod animals - inter-leg coordination in free-

walking adult stick insects," *J Exp Biol*, vol. 215, no. Pt 24, pp. 4255-66, 2012.

[42] R.B. McGhee, A.A. Frank, "On the stability properties of quadruped creeping gaits," *Mathematical Biosciences*, vol. 3, pp. 331-351, 1968.

[43] N. Ma, J. Yu, X. Dong, and D. Axinte, "Design and stiffness analysis of a class of 2-DoF tendon driven parallel kinematics mechanism," *Mechanism and Machine Theory*, vol. 129, pp. 202-217, 2018.



Josue Camacho-Arreguin received the B.Eng. in aeronautical engineering from I.P.N, Mexico in 2013; and the M.Eng. degree in aeronautical engineering by U.A.N.L, Mexico in 2016. He is currently working towards the Ph.D. degree in mechanical engineering at the University of Nottingham, working on parallel mechanisms for in-situ repair and maintenance. His research interests are mechanical design, structural analysis and robotics.



Mingfeng Wang received the B.Eng. degree in mechanical design and automation and the M. Eng. Degree in mechanical engineering from Central South University, Changsha, China, in 2008 and 2012, respectively and the PhD degree in mechanical engineering from University of Cassino and South Latium Italy in 2016. He is currently a Research Fellow at Rolls-Royce University Technology Centre (UTC), University of Nottingham, UK. His research interests cover humanoid robots, precision farming robots,

continuum robots.



Matteo Russo (M'18) received the B.Sc., M.Sc. and Ph.D. degrees in mechanical engineering from the University of Cassino, Italy, in 2013, 2015, and 2019, respectively. Between 2015 and 2017 he was a visiting researcher at RWTH Aachen University, University of the Basque Country and Tokyo Institute of Technology.

Since 2019, he is a Research Fellow at the Rolls-Royce UTC in Manufacturing and On-Wing Technology, University of Nottingham, Nottingham, UK. His main research interests are continuum robots, robot kinematics and parallel manipulators.



Xin Dong received his B. Eng. Degree in mechanical engineering from Dalian University of Technology, Dalian, China 2008, the M. Eng and PhD degrees in Mechatronics, Robotics and Automation Engineering from Beihang University, Beijing, China in 2011 and from University of Nottingham, Nottingham, UK, 2015.

He is currently an Assistant Professor working at the University of Nottingham. His research interests are extra slender continuum robot and reconfigurable hexapod robots with novel actuation solutions for the application in Aerospace, Nuclear, Oil & Gas, Marine and rescue.



Dragos Axinte received the M.Eng. degree in manufacturing engineering in 1988, and the Ph.D. degree in manufacturing engineering in 1996.

After graduating, he worked in R&D in industry for 10 years and then moved to academia to lead research in the field of machining, process monitoring and design of innovative tooling/robotics for in-situ repair especially related to on-wing repair of aeroengines.

Currently, he is Professor of Manufacturing Engineering at University of Nottingham and Director of Rolls-Royce University Technology Centre (UTC) in Manufacturing and On-Wing Technology.